Benchmark study of an auxiliary-field quantum Monte Carlo technique for the Hubbard model with shifted-discrete Hubbard-Stratonovich transformations

Kazuhiro Seki[1,2,3] and Sandro Sorella[1,2,4]

[1]*Scuola Internazionale Superiore di Studi Avanzati, via Bonomea, 265-34136 Trieste, Italy*

[2]*Computational Materials Science Research Team, RIKEN Center for Computational Science (R-CCS), Kobe, Hyogo 650-0047, Japan*

[3]*Computational Condensed Matter Physics Laboratory, RIKEN, Wako, Saitama 351-0198, Japan*

[4]*Democritos Simulation Center, CNR–IOM Istituto Officina dei Materiali, Via Bonomea 265, 34136 Trieste, Italy*

(Received 23 January 2019; revised manuscript received 18 March 2019; published 8 April 2019)

Within the ground-state auxiliary-field quantum Monte Carlo technique, we introduce discrete Hubbard-Stratonovich transformations (HSTs) that are also suitable for spatially inhomogeneous trial functions. The discrete auxiliary fields introduced here are coupled to local spin or charge operators fluctuating around their Hartree-Fock values. The formalism can be considered a generalization of the discrete HSTs by J. E. Hirsch [Phys. Rev. B **28**, 4059 (1983)] or a compactification of the shifted-contour auxiliary-field Monte Carlo formalism by N. Rom *et al.* [Chem. Phys. Lett. **270**, 382 (1997)]. An improvement of the acceptance ratio is found for a real auxiliary field, while an improvement of the average sign is found for a purely imaginary auxiliary field. Efficiencies of the different HSTs are tested in the single-band Hubbard model at and away from half filling by studying the staggered magnetization and energy expectation values, respectively.

DOI: 10.1103/PhysRevB.99.144407

I. INTRODUCTION

The numerical solution of the Hubbard model with strong correlations is one of the most challenging issues in the theory of strongly correlated electron systems [1,2]. Attempts to determine the ground state are often based on iterative techniques based on a repeated application of a short imaginary-time propagator or using the simple power method and more advanced Krylov-subspace techniques, such as the Lanczos algorithm, where a Hamiltonian operator is repeatedly applied to a properly chosen trial state. In both cases the ground-state component of the trial state is filtered out after several iterations.

Among these projection techniques, the auxiliary-field quantum Monte Carlo (AFQMC) [3–6] is one of the most powerful schemes, as it allows us to study, for example, the ground-state properties of the Hubbard model with several thousand electrons and lattice sites when the negative-sign problem is absent [7–9]. In the ground-state AFQMC, even if the Hamiltonian is the same, there exists some arbitrariness in choosing the trial wave function and the type of auxiliary fields (e.g., real, complex, continuous, or discrete). Experience has shown that an appropriate choice of these ingredients may significantly improve the efficiency of the Monte Carlo simulations [10].

It has been demonstrated [2,11] that a Slater determinant obtained from an unrestricted Hartree-Fock (UHF) approximation [12] provides a good trial wave function for the doped Hubbard model in the constrained-path AFQMC [13]. Recently, for a particular parameter set at doping $\delta = 1/8$ and electron-electron repulsion $U/t = 8$, the ground state of the Hubbard model on the square lattice was predicted to exhibit a vertical stripe order [2], where the stripe states with periods $\lambda = 5, 6, 7$, and 8 in units of the lattice constant are nearly degenerate, while a spatially homogeneous d-wave superconducting state should have, according to their study, a higher energy. Recent variational Monte Carlo (VMC) calculations [14–16] have also shown that various vertical-stripe orders with different periods appear, depending on the doping and the hopping parameter. In most of the calculations in Ref. [2], the symmetry of finite-size clusters is broken due to the use of UHF trial wave functions or by applying pinning magnetic fields, and the results are extrapolated to the thermodynamic limit. The success of utilizing symmetry-broken wave functions is rather surprising because symmetry breakings do not occur in the exact ground state of finite-size systems. A similar issue is known as the symmetry dilemma in first-principles calculations for molecules [17,18]. Recently, it was shown that the quality of the trial wave function can be improved by restoring the symmetries that are broken by UHF or mean-field treatments [19–21]. However, in the present work, we do not enter into the issue of symmetry breakings of trial wave functions, but rather focus on the arbitrariness of the auxiliary field to improve the efficiency of AFQMC simulations with such symmetry-broken trial wave functions.

The way of transforming a quartic interaction term into a quadratic one via the Hubbard-Stratonovich transformation (HST) [22] is not unique and affects the efficiency of simulations [23–28]. Recently, the popularity of this technique has substantially increased because it has been realized that, with continuous auxiliary fields, one can treat interaction terms beyond the on-site Hubbard interaction, up to the complete treatment of the long-range Coulomb interaction [29–34] or of the long-range electron-phonon interaction [35] or even both of them on the same footing [36], without being vexed by the sign problem in a certain parameter region on bipartite lattices. Interestingly, such a parameter region coincides with the one where rigorous statements on the ground state of an

extended Hubbard-Holstein model are available [37,38]. It is also noteworthy that, even when the sign problem cannot be eliminated completely, continuous auxiliary fields with a proper shift [39–41] can improve the efficiency of simulations compared to one without the shift. A similar idea was also employed in the AFQMC [42,43] within the constrained-path approximation [13].

In this paper, we introduce shifted-discrete HSTs, where auxiliary fields are coupled to the fluctuation of local spin or charge. The method is applied to AFQMC simulations of the Hubbard model on the square lattice. It is shown that the shifted-discrete HSTs can improve the efficiency of the AFQMC simulations. Moreover, we present results on the magnetic order parameter as a function of U/t with high statistical accuracy, which represents an important benchmark and is also useful for comparison with experiments.

The rest of this paper is organized as follows. In Sec. II, the Hubbard model is defined, and the AFQMC method is described. In Sec. III, the shifted-discrete HSTs are introduced. In Sec. IV, numerical results of the AFQMC simulations for the Hubbard model are presented. Section V is devoted to conclusions and discussion.

II. MODEL AND METHOD

We consider the Hubbard model whose Hamiltonian is defined by $\hat{H} = \hat{K} + \hat{V}$, where

$$\hat{K} = -t \sum_{\langle ij\rangle,\sigma} (\hat{c}^{\dagger}_{i\sigma}\hat{c}_{j\sigma} + \text{H.c.}), \tag{1}$$

$$\hat{V} = U \sum_{i} \hat{n}_{i\uparrow}\hat{n}_{i\downarrow}, \tag{2}$$

$\hat{c}^{\dagger}_{i\sigma}$ ($\hat{c}_{i\sigma}$) creates (annihilates) a fermion with site index i and spin index σ ($=\uparrow,\downarrow$), $\hat{n}_{i\sigma} = \hat{c}^{\dagger}_{i\sigma}\hat{c}_{i\sigma}$, t is the hopping parameter between the nearest-neighbor sites on the square lattice, and $U > 0$ is the on-site electron-electron repulsion. We consider the Hubbard model on $N = L \times L$ site clusters. Boundary conditions will be specified for each calculation in Sec. IV. The lattice constant is set to be unity.

In the AFQMC, the expectation value of an operator $\hat{O}$ is calculated as

$$\langle \hat{O} \rangle_{\beta} = \frac{\langle \Psi_{\mathrm{T}} | e^{-\frac{\beta}{2}\hat{H}} \hat{O} e^{-\frac{\beta}{2}\hat{H}} | \Psi_{\mathrm{T}} \rangle}{\langle \Psi_{\mathrm{T}} | e^{-\beta\hat{H}} | \Psi_{\mathrm{T}} \rangle}, \tag{3}$$

where β is the projection time and $|\Psi_{\mathrm{T}}\rangle$ is a trial wave function. If β is infinitely large, one can obtain the ground-state expectation value as long as $|\Psi_{\mathrm{T}}\rangle$ has a finite overlap with the ground state [44]. If β is finite, the results depend on the trial wave function (see, for example, Ref. [45]). If $\beta = 0$, Eq. (3) reduces to the expectation value of $\hat{O}$ with respect to the trial wave function.

At finite dopings, $|\Psi_{\mathrm{T}}\rangle$ is obtained by solving the eigenvalue problem of the following UHF Hamiltonian self-consistently:

$$\hat{H}_{\mathrm{UHF}} = \hat{K} + U_{\mathrm{eff}} \sum_{i} (\langle \hat{n}_{i\uparrow}\rangle_0 \hat{n}_{i\downarrow} + \hat{n}_{i\uparrow}\langle \hat{n}_{i\downarrow}\rangle_0 - \langle \hat{n}_{i\uparrow}\rangle_0 \langle \hat{n}_{i\downarrow}\rangle_0), \tag{4}$$

where U_{eff} is an arbitrary parameter and the expectation value $\langle \cdots \rangle_0$ in Eq. (4) is defined in Eq. (3) with $\beta = 0$. A fine tuning of U_{eff} can improve the quality of the trial wave function [11]. We set $U_{\mathrm{eff}}/t = 2.5$, which has turned out to provide a good trial wave function for the doped cases studied here in the sense that the energy expectation value decreases quickly with increasing β. By adding a small bias in the initial condition for the self-consistent UHF loop to pin the direction of the stripe, $|\Psi_{\mathrm{T}}\rangle$ shows a vertical stripe order with period $\lambda = 8$ around $\delta = 1/8$ doping on the 16×16 cluster.

At half filling, $|\Psi_{\mathrm{T}}\rangle$ is obtained as a ground state of non-interacting electrons on the square lattice under a staggered magnetic field along the spin-quantized axis (z direction):

$$\hat{H}_{\mathrm{MF}} = \hat{K} - \Delta_{\mathrm{AF}} \sum_{i} (-1)^i (\hat{n}_{i\uparrow} - \hat{n}_{i\downarrow}), \tag{5}$$

where $(-1)^i = 1$ (-1) if site i belongs to the A (B) sublattice and Δ_{AF} can be chosen arbitrarily. The value of Δ_{AF} will be specified with the numerical results in Sec. IV.

By using the second-order Suzuki-Trotter decomposition [46,47], the imaginary-time propagator can be expressed as

$$e^{-\beta\hat{H}} = \prod_{l=1}^{N_\tau} \left(e^{-\frac{\Delta_\tau}{2}\hat{K}} e^{-\Delta_\tau \hat{V}} e^{-\frac{\Delta_\tau}{2}\hat{K}} \right) + O(\Delta_\tau^2), \tag{6}$$

where the projection time β is discretized into N_τ time slices and $\Delta_\tau = \beta/N_\tau$. For the doped cases, we set $\Delta_\tau t = 0.05$ so that the discretization error is within statistical errors. For the half-filled case, we perform extrapolations of $\Delta_\tau \to 0$ to eliminate the discretization error, which becomes non-negligible for large U/t compared to statistical or extrapolation errors for the results shown in Sec. IV B. An HST is applied to $e^{-\Delta_\tau \hat{V}}$, and the summation over auxiliary fields is performed using the Monte Carlo method with the importance sampling, where a proposed auxiliary-field configuration is accepted or rejected according to the Metropolis algorithm. Details of the importance sampling method within the AFQMC are given in Appendix A. In the next section, we introduce shifted-discrete HSTs for $e^{-\Delta_\tau \hat{V}}$.

III. SHIFTED-DISCRETE HUBBARD-STRATONOVICH TRANSFORMATIONS

In this section we derive shifted-discrete HSTs which couple the auxiliary field to the local spin fluctuation in Sec. III A and to the local charge fluctuation in Sec. III B. Although the two HSTs can be formulated almost in parallel, we provide both of them separately for completeness.

A. Auxiliary field coupled to spin fluctuation

The Hubbard interaction in Eq. (2) can be written as

$$\hat{V} = -\frac{U}{2} \sum_{i} \left[(\hat{n}_{i\uparrow} - \hat{n}_{i\downarrow} - \tilde{m}_i)^2 - \tilde{m}_i^2 \right] + \frac{U}{2} \sum_{i} \left[(1 - 2\tilde{m}_i)\hat{n}_{i\uparrow} + (1 + 2\tilde{m}_i)\hat{n}_{i\downarrow} \right], \tag{7}$$

where $\tilde{m}_i$ is an arbitrary number. Then $e^{-\Delta_\tau V}$ can be written as

$$e^{-\Delta_\tau \hat{V}} = e^{\frac{\Delta_\tau U}{2}\sum_i[(\hat{n}_{i\uparrow}-\hat{n}_{i\downarrow}-\tilde{m}_i)^2-\tilde{m}_i^2]} \times e^{-\frac{\Delta_\tau U}{2}\sum_i(1-2\tilde{m}_i)\hat{n}_{i\uparrow}} e^{-\frac{\Delta_\tau U}{2}\sum_i(1+2\tilde{m}_i)\hat{n}_{i\downarrow}}. \quad (8)$$

Let us consider the first exponential factor on the right-hand side of Eq. (8). For each site i, we consider the following HST:

$$C_i e^{-\frac{\Delta_\tau U}{2}\tilde{m}_i^2} e^{\frac{\Delta_\tau U}{2}(\hat{n}_{i\uparrow}-\hat{n}_{i\downarrow}-\tilde{m}_i)^2} = \frac{1}{2}\sum_{s_i=\pm1} e^{\alpha_i s_i(\hat{n}_{i\uparrow}-\hat{n}_{i\downarrow}-m_i)}, \quad (9)$$

where $s_i = \pm 1$ is the discrete auxiliary field and the four undetermined parameters α_i, m_i, $\tilde{m}_i$, and C_i are related through the following three equations (see Appendix B for a derivation):

$$\frac{\cosh\alpha_i(1-m_i)\cosh\alpha_i(1+m_i)}{\cosh^2\alpha_i m_i} = e^{\Delta_\tau U}, \quad (10)$$

$$\tilde{m}_i = \frac{1}{2\Delta_\tau U}\ln\frac{\cosh\alpha_i(1+m_i)}{\cosh\alpha_i(1-m_i)}, \quad (11)$$

$$C_i = e^{\Delta_\tau U\tilde{m}^2/2}\cosh\alpha_i m_i. \quad (12)$$

Therefore, if, say, m_i is given, α_i, $\tilde{m}_i$, and C_i are determined from Eqs. (10)–(12). Finally, we obtain

$$e^{-\Delta_\tau \hat{V}} \propto \prod_i \sum_{s_i=\pm1} e^{[\alpha_i s_i - \frac{\Delta_\tau U}{2}(1-2\tilde{m}_i)]\hat{n}_{i\uparrow} + [-\alpha_i s_i - \frac{\Delta_\tau U}{2}(1+2\tilde{m}_i)]\hat{n}_{i\downarrow} - \alpha_i s_i m_i}. \quad (13)$$

Note that, in general, $m_i \neq \tilde{m}_i$ and C_i are irrelevant for results of simulations because they cancel out from the numerator and the denominator in Eq. (3). If $m_i = 0$, the HST reduces to the one introduced by Hirsch [23]. However, the arbitrariness of m_i can be utilized to improve the efficiency of AFQMC simulations, as shown in Sec. IV.

On the right-hand side of Eq. (13), the auxiliary field $\alpha_i s_i$ is shifted by $\Delta_\tau U\tilde{m}_i$ compared to the case of $m_i = \tilde{m}_i = 0$. To obtain more physical intuitions for m_i, we rewrite the exponent on the right-hand side of Eq. (13) as

$$\alpha_i s_i(\hat{n}_{i\uparrow}-\hat{n}_{i\downarrow}-m_i) + \Delta_\tau U\tilde{m}_i(\hat{n}_{i\uparrow}-\hat{n}_{i\downarrow}) - \frac{\Delta_\tau U}{2}(\hat{n}_{i\uparrow}+\hat{n}_{i\downarrow}). \quad (14)$$

In the first term, the auxiliary field $\alpha_i s_i$ is coupled to the fluctuation of the local magnetization $(\hat{n}_{i\uparrow}-\hat{n}_{i\downarrow}-m_i)$, while the shift of the local magnetization by $-m_i$ in the first term is compensated by the spatially inhomogeneous magnetic field $\Delta_\tau U\tilde{m}_i$ in the second term.

We set the parameter m_i as the local magnetization in the trial wave function,

$$m_i = \langle\hat{n}_{i\uparrow}-\hat{n}_{i\downarrow}\rangle_0. \quad (15)$$

This m_i can easily be calculated and is expected to stabilize the simulation by keeping the first term in Eq. (14) "small" during the imaginary-time evolution. For a given m_i, α_i can be determined from Eq. (10), $\tilde{m}_i$ can be determined from Eq. (11), and C_i can be determined from Eq. (12). The solution α_i of Eq. (10) can be found with the Newton method with an initial guess $\alpha_{i,\text{initial}} = \cosh^{-1} e^{\Delta_\tau U/2}$, for example.

B. Auxiliary field coupled to charge fluctuation

In this section, α_i and C_i will be redefined. The Hubbard interaction in Eq. (2) can be written as

$$\hat{V} = \frac{U}{2}\sum_i\left[(\hat{n}_{i\uparrow}+\hat{n}_{i\downarrow}-\tilde{n}_i)^2-\tilde{n}_i^2\right] - \frac{U}{2}\sum_i[(1-2\tilde{n}_i)\hat{n}_{i\uparrow}+(1-2\tilde{n}_i)\hat{n}_{i\downarrow}], \quad (16)$$

where $\tilde{n}_i$ is an arbitrary number. Then $e^{-\Delta_\tau V}$ can be written as

$$e^{-\Delta_\tau \hat{V}} = e^{-\frac{\Delta_\tau U}{2}\sum_i[(\hat{n}_{i\uparrow}+\hat{n}_{i\downarrow}-\tilde{n}_i)^2-\tilde{n}_i^2]} \times e^{\frac{\Delta_\tau U}{2}\sum_i(1-2\tilde{n}_i)\hat{n}_{i\uparrow}} e^{\frac{\Delta_\tau U}{2}\sum_i(1-2\tilde{n}_i)\hat{n}_{i\downarrow}}. \quad (17)$$

Let us consider the first exponential factor on the right-hand side of Eq. (17). For each site i, we consider the following HST:

$$C_i e^{\frac{\Delta_\tau U}{2}\tilde{n}_i^2} e^{-\frac{\Delta_\tau U}{2}(\hat{n}_{i\uparrow}+\hat{n}_{i\downarrow}-\tilde{n}_i)^2} = \frac{1}{2}\sum_{s_i=\pm1} e^{i\alpha_i s_i(\hat{n}_{i\uparrow}+\hat{n}_{i\downarrow}-n_i)}, \quad (18)$$

where $s_i = \pm 1$ is the discrete auxiliary field and the four undetermined parameters α_i, n_i, $\tilde{n}_i$, and C_i are related through the following three equations (see Appendix B for derivation):

$$\frac{\cos\alpha_i(2-n_i)\cos\alpha_i n_i}{\cos^2\alpha_i(1-n_i)} = e^{-\Delta_\tau U}, \quad (19)$$

$$\tilde{n}_i = 1 - \frac{1}{2\Delta_\tau U}\ln\frac{\cos\alpha_i n_i}{\cos\alpha_i(2-n_i)}, \quad (20)$$

$$C_i = e^{-\Delta_\tau U\tilde{n}_i^2/2}\cos\alpha_i n_i. \quad (21)$$

Therefore, if, say, n_i is given, α_i, $\tilde{n}_i$, and C_i are determined from Eqs. (19)–(21). Finally, we obtain

$$e^{-\Delta_\tau \hat{V}} \propto \prod_i \sum_{s_i=\pm1} e^{\left[i\alpha_i s_i + \frac{\Delta_\tau U}{2}(1-2\tilde{n}_i)\right]\hat{n}_{i\uparrow} + \left[i\alpha_i s_i + \frac{\Delta_\tau U}{2}(1-2\tilde{n}_i)\right]\hat{n}_{i\downarrow} - i\alpha s_i n_i}. \quad (22)$$

Note that, in general, $n_i \neq \tilde{n}_i$ and C_i are irrelevant for the results of simulations because they cancel out between the numerator and the denominator in Eq. (3). If $n_i = 1$, the HST reduces to the one introduced by Hirsch [23]. However, the arbitrariness of n_i can be utilized to improve the efficiency of AFQMC simulations, as shown in Sec. IV.

On the right-hand side of Eq. (22), the auxiliary field $i\alpha_i s_i$ is shifted by $\Delta_\tau U(1-\tilde{n}_i)$ compared to the case of $n_i = \tilde{n}_i = 1$. To obtain more physical intuitions for n_i, we rewrite the exponent on the right-hand side of Eq. (22) as

$$i\alpha_i s_i(\hat{n}_{i\uparrow}+\hat{n}_{i\downarrow}-n_i) + \Delta_\tau U(1-\tilde{n}_i)(\hat{n}_{i\uparrow}+\hat{n}_{i\downarrow}) - \frac{\Delta_\tau U}{2}(\hat{n}_{i\uparrow}+\hat{n}_{i\downarrow}). \quad (23)$$

In the first term, the auxiliary field $i\alpha_i s_i$ is coupled to the fluctuation of the local density $(\hat{n}_{i\uparrow}+\hat{n}_{i\downarrow}-n_i)$, while the shift of the local density by $-(1-n_i)$ in the first term is compensated by the spatially inhomogeneous chemical potential $\Delta_\tau U(1-\tilde{n}_i)$ in the second term.

We set the parameter n_i as the local charge density in the trial wave function

$$n_i = \langle \hat{n}_{i\uparrow} + \hat{n}_{i\downarrow} \rangle_0. \tag{24}$$

This n_i can easily be calculated and is expected to stabilize the simulation by keeping the first term in Eq. (23) "small" during the imaginary-time evolution. For a given n_i, α_i can be determined from Eq. (19), $\tilde{n}_i$ can be determined from Eq. (20), and C_i can be determined from Eq. (21). The solution α_i of Eq. (19) can be found with the Newton method with an initial guess $\alpha_{i,\text{initial}} = \cos^{-1} e^{-\Delta_\tau U/2}$, for example.

IV. NUMERICAL RESULTS

A. Finite dopings

At finite dopings, the sign problem occurs [48,49]. In the presence of the sign problem, the projection time β cannot be taken to be as large as that for the half-filled case because the average sign (of the statistical weight) decreases exponentially in β [49]; otherwise, the number of statistical samplings has to be increased exponentially to keep the statistical error small. We set the maximum β as the one at which the average sign is $\sim$0.05. It will be shown that even in the presence of the sign problem, the AFQMC can still provide a good upper bound of the ground-state energy.

Figure 1 shows the energy per site $E(\beta) = \langle \hat{H} \rangle_\beta / N$, the acceptance ratio, and the average sign as a function of β at $U/t = 8$ for the 16×16 cluster with 224 electrons, corresponding to $\delta = 1/8 = 0.125$. Note that since

$$\frac{dE(\beta)}{d\beta} = -\frac{1}{N}\left(\langle \hat{H}^2 \rangle_\beta - \langle \hat{H} \rangle_\beta^2\right) \leqslant 0, \tag{25}$$

$E(\beta)$ is a decreasing function of β and its slope $dE(\beta)/d\beta$ is proportional to the energy variance [44]. The energies calculated by different HSTs in Fig. 1(a) coincide within the statistical errors because the same imaginary-time-evolution operator in Eq. (6) is applied to the same trial wave function $|\Psi_T\rangle$. However, their reachable β is different because the average sign, shown in Fig. 1(b), can depend on the choice of the HST. In Fig. 1(c), the acceptance ratio of the real auxiliary field with the shift (HST spin with shift) is increased from the one without the shift (HST spin without shift). The reason can be attributed to the fact that since the first term of Eq. (14) with a relevant m_i is expected to be smaller than that with $m_i = 0$, the factor $e^{\pm 2\alpha_i(\hat{n}_{i\uparrow} - \hat{n}_{i\downarrow} - m_i)}$ is closer to unity. Therefore, the fluctuation of the modulus of the determinant ratio is stabilized [see Eqs. (A3) and (A9)]. On the other hand, the shift of the real auxiliary field does not affect the average sign significantly because the shift does not affect the sign of the determinant [see Eqs. (A3) and (A7)], as can be seen in Fig. 1(b). We have found that the increased acceptance ratio corresponds to a more efficient statistical sampling because several quantities—such as energy, kinetic energy, and double occupancy—can be obtained with smaller statistical errors at a given computational time.

The situation is different for the purely imaginary auxiliary fields. Without the shift (HST charge without shift), the average sign diminishes significantly, even at $\beta t = 0.1$. By introducing the shift (HST charge with shift), the average sign is improved significantly. The reason can be attributed to the fact that since the first term in Eq. (23) with a relevant n_i is expected to be smaller than that with $n_i = 1$, the factor $e^{\pm 2i\alpha_i(\hat{n}_{i\uparrow} + \hat{n}_{i\downarrow} - n_i)}$ is closer to unity. Therefore, the fluctuation of the phase of the determinant is stabilized. Although the average sign is still quite smaller than that obtained with the real auxiliary fields, our results suggest that in more general cases, for instance, with genuinely complex fields [23,50], the proposed technique may provide an improvement in the sampling.

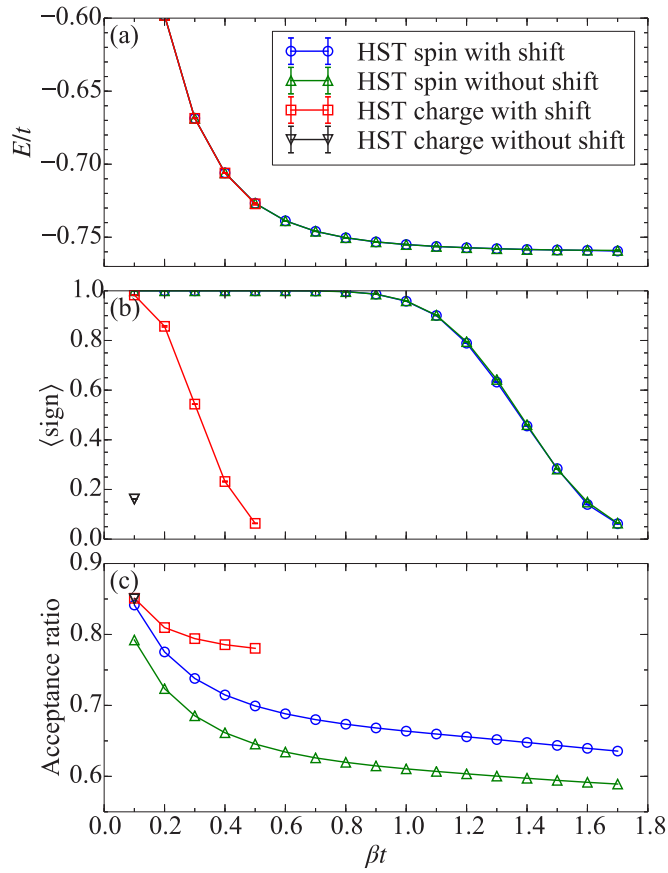

FIG. 1. (a) The energy per site, (b) the average sign, and (c) the acceptance ratio as a function of the projection time β with different HSTs. Calculations are done on the 16×16 cluster with 224 electrons ($\delta = 0.125$) at $U/t = 8$.

To show the usefulness of the AFQMC with a short imaginary-time propagation, we make a comparison with the state-of-the-art variational wave functions for the Hubbard model [14,15]. To this end, we move to the smaller doping with the larger U/t, where the more severe sign problem is expected. Figure 2 shows the energy per site and the average sign as a function of β at $U/t = 10$ for the 16×16 cluster with 228 electrons, corresponding to $\delta = 0.109375$. Here, only the shifted real auxiliary field is employed because it turned out to be the most efficient, as shown in Fig. 1 for $U/t = 8$ and $\delta = 0.125$. We use periodic (antiperiodic) boundary conditions in the x (y) direction to compare our results directly with the reference VMC results [14,15]. Notice that our AFQMC energy, computed at finite projection time β when the average sign is sufficiently large, respects Ritz's variational principle [see Eq. (3)] because it corresponds to the variational expectation

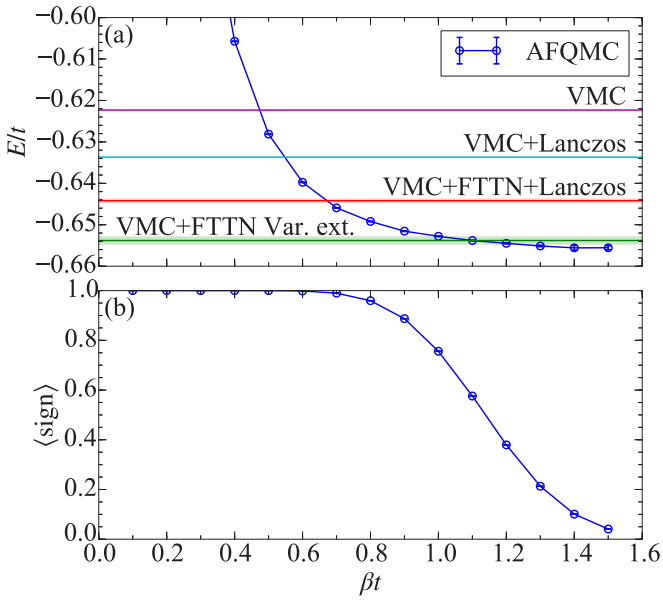

FIG. 2. (a) The energy per site and (b) the average sign as a function of the projection time β. Calculations refer to the 16×16 cluster with 228 electrons ($\delta = 0.109375$) at $U/t = 10$. In (a), the horizontal lines and the shaded regions are the VMC energies, and their error bars are taken from Refs. [14,15]. FTTN stands for fat-tree tensor network, and Var. ext. stands for variance extrapolation.

value of $\hat{H}$ over the state $e^{-\frac{\beta}{2}\hat{H}}|\Psi_T\rangle/\langle\Psi_T|e^{-\beta\hat{H}}|\Psi_T\rangle^{\frac{1}{2}}$. This is a useful property of an approximate technique that is not always satisfied, for instance, for the constrained-path AFQMC [13,42]. At $\beta t = 0.7$, where the average sign remains ∼0.99, the AFQMC energy is already lower than the VMC energy without variance extrapolation. At $\beta t = 1.1$, the AFQMC energy almost coincides with the VMC variance-extrapolated one, while the slope $dE(\beta)/d\beta$ is still finite, indicating that the AFQMC energy variance is nonzero [see Eq. (25)]. At $\beta t = 1.5$, the AFQMC energy is $E/t = -0.6552(4)$, which is lower than the variance-extrapolated VMC energy $E/t = 0.6538(9)$ [14], which may be compatible with our number within two standard deviations. This result suggests that the ground-state AFQMC method remains very useful for providing upper-bound values of the ground-state energy even in the presence of the negative-sign problem.

B. Half filling

At half filling, the sign problem is absent. Therefore, the AFQMC can provide exact results which often serve as a reference benchmark for other numerical techniques. Excellent agreement in the ground-state energies of the two-dimensional Hubbard model between the AFQMC and other many-body techniques was reported in Ref. [1]. Moreover, within the AFQMC, the staggered magnetization m, i.e., the order parameter at half filling, can be estimated accurately by using the twist-averaged boundary condition for small U/t, e.g., $U \lesssim 4$ [51,52]. However, for large U/t, AFQMC simulations still face the difficulty of large fluctuations of the magnetization, which often lead to a relatively large error bar in m [1,51]. The same difficulty also arises in finite-temperature determinant

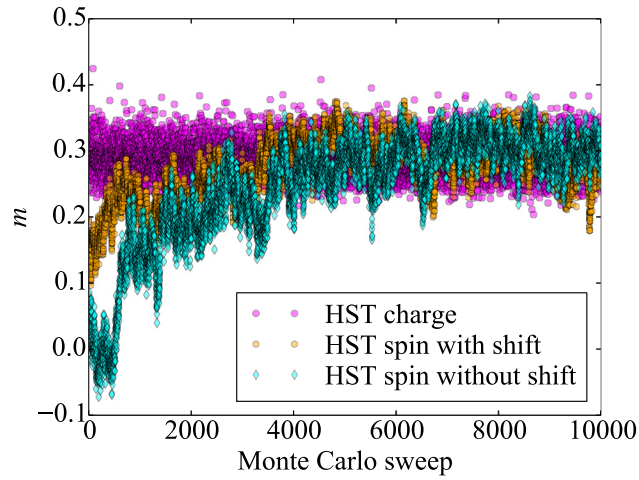

FIG. 3. The staggered magnetization m as a function of the Monte Carlo sweep for the half-filled Hubbard model on the square lattice at $U/t = 8$ with different HSTs. Calculations are done on the 16×16 cluster with $\beta t = 24$.

QMC simulations [53,54]. In previous works, in order to overcome the difficulty, a pinning-field method was proposed, with a clear improvement for the determination of m in the thermodynamic limit [55,56]. In the following, we report an accurate estimate m, especially for large U/t, by making use of a symmetry-broken trial wave function.

Figure 3 shows the staggered magnetization along the z direction,

$$m(\beta) = \frac{1}{2N}\sum_i (-1)^i \langle \hat{n}_{i\uparrow} - \hat{n}_{i\downarrow}\rangle_\beta, \tag{26}$$

as a function of the Monte Carlo sweep with different HSTs. The calculations are done for $U/t = 8$, $\beta t = 24$, and $\Delta_\tau t = 0.1$ on the $L = 16$ cluster with periodic boundary conditions. We use $\Delta_{AF}/t = 0.001$ to give a finite staggered magnetization in the trial wave function. This small value of Δ_{AF} is effective for pinning a sizable value of the finite-size order parameter $m(0)$ because the single-particle states at $U/t = 0$ have a large degeneracy ($\propto L$) at the Fermi level and are therefore strongly renormalized upon an arbitrarily small Δ_{AF}.

Since $m(0)$ is finite [see Eq. (5)], $m(\beta)$ remains finite even for finite L. Note that at half filling, the HST in the charge channel with shift is equivalent to the one without shift because $n_i = 1$. A very large equilibration time of ∼5000 Monte Carlo sweeps is found for m with the standard real HST coupled to the on-site electron spins. In this case, our shifted HST improves the equilibration time, allowing also a higher acceptance ratio (not shown) as in the doped cases, but the improvement is not really important. Amazingly, m is equilibrated almost immediately for the complex HST coupled to the on-site electron charges. This result implies that this purely imaginary auxiliary field, which was first introduced by Hirsch [23], is very useful to estimate m at half filling for large U/t. Here, we also emphasize that not only is the correlation time highly reduced with this technique, but also the fluctuations, thanks to this pinning strategy in the trial wave function, do not show any problem of large fluctuations, even at very large U/t and values.

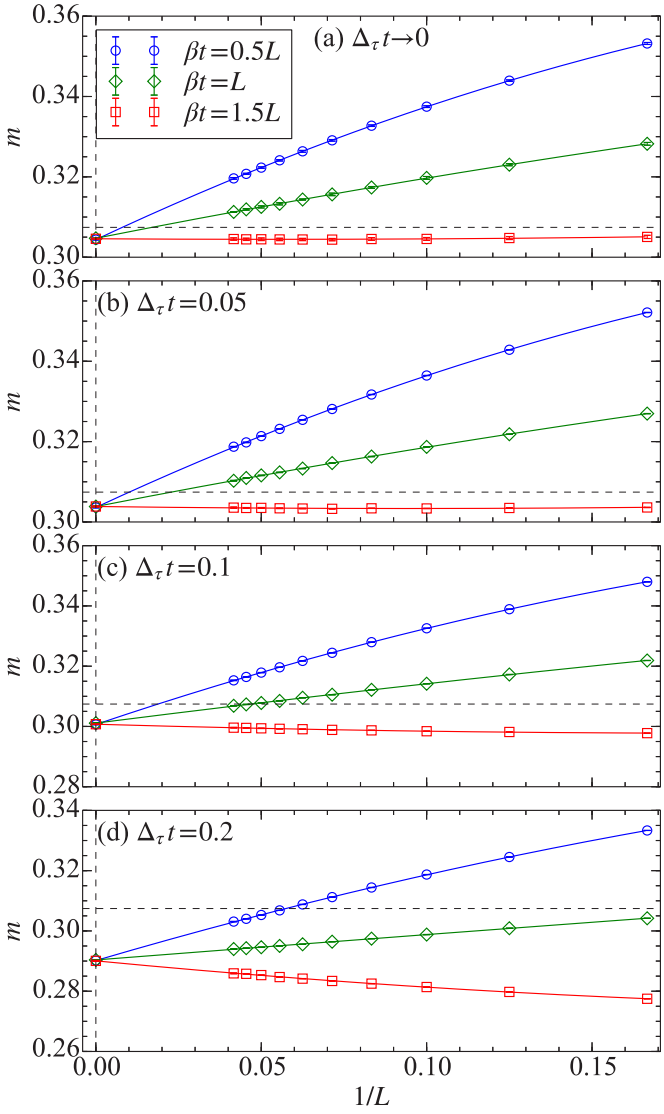

FIG. 4. Finite-size scaling of the staggered magnetization m of the half-filled Hubbard model at $U/t = 10$ with $\beta t = 0.5L$, L, and $1.5L$ for (a) $\Delta_\tau t \to 0$, (b) $\Delta_\tau t = 0.05$, (c) $\Delta_\tau t = 0.1$, and (d) $\Delta_\tau t = 0.2$. The dashed horizontal lines indicate m of the Heisenberg model in the thermodynamic limit taken from Ref. [61].

Figure 4 shows the finite-size scaling of m for $U/t = 10$. The cluster sizes used are $L = 6$, 8, 10, 12, 14, 16, 18, 20, 22, and 24. Here, the projection time β is chosen to be proportional to L, i.e., $\beta t = \alpha L$, with $\alpha = 0.5$, 1, and 1.5. These βt values are an order of magnitude smaller than those used with the pinning-field method [55,56] because in our approach we can reach the thermodynamic limit consistently without unnecessarily large values of β. Indeed, the extrapolated values at $1/\beta = 1/L = 0$ are consistent for all values of α, which validates our approach. Our best estimate is obtained from the $\beta t = 1.5L$ set of data, yielding $m = 0.3046(1)$ in the $\Delta \to 0$ limit, where the number in the parentheses indicates the extrapolation error in the last digit. Calculations are done for $\Delta_\tau t = 0.2$, 0.1, and 0.05, and the extrapolations to $\Delta_\tau \to 0$ are obtained by a linear fit in $(\Delta_\tau t)^2$, determined by the least-squares method. The ground-state expectation value m in the thermodynamic limit is obtained by extrapolating the results to $L \to \infty$. In this case we fit the data in the range $6 \leqslant L \leqslant 24$ with quadratic polynomials in $1/L$. As can be seen in Fig. 4, the time-discretization error is not negligible for $U/t = 10$. The extrapolated value is certainly smaller than the one in the Heisenberg model [57–60], where the latest Monte Carlo estimate is $m = 0.30743(1)$ [61,62].

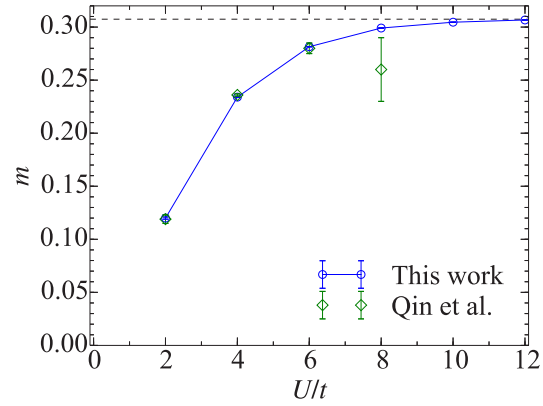

FIG. 5. The staggered magnetization m in the thermodynamic limit as a function of U. For comparison, previous AFQMC results are taken from Ref. [11]. The dashed horizontal line indicates m of the Heisenberg model in the thermodynamic limit taken from Ref. [61].

In Table I and Fig. 5 we show the values of m in the thermodynamic limit for $U/t = 2$, 4, 6, 8, 10, and 12 and compare them with the ones available in the literature [36,51,52,63]. The main outcome of this work is the estimated value of m for $U/t \geqslant 8$, which is usually the accepted value for cuprates. Here, our error bar at $U/t = 8$ is two orders of magnitude smaller than the previous AFQMC estimate [1,51]. Thanks to this high statistical accuracy, our results clearly show that m increases monotonically in U/t. This is consistent with a strong-coupling expansion around the Heisenberg limit [64]. Here, finite-size scaling analyses are performed as follows. For $U/t \geqslant 6$, the scheme of finite-size scaling analyses is the same as that for $U/t = 10$, which has been described before. For $U/t = 4$ ($U/t = 2$), cluster sizes up to $L = 32$ ($L = 50$) with twist-averaged boundary conditions [51,52,65–68] are used because the finite-size effects are more important than those we have found at larger U/t values. A much larger value of $\Delta_{\rm AF}/t = 10$ is used for $U/t \leqslant 4$ because the twists remove the degeneracy of the single-particle states at $U/t = 0$, as discussed before. All the results are obtained in the $\Delta_\tau \to 0$ limit using data at $\Delta_\tau t = 0.2$, 0.1, and 0.05 for $U/t \geqslant 4$ and $\Delta_\tau t = 0.25$, 0.2, and 0.1 for $U/t = 2$.

V. CONCLUSIONS AND DISCUSSION

In this work we have shown that, within the ground-state AFQMC technique, the choice of the trial function and the one for the auxiliary field are extremely important. In particular we have improved the efficiency of the method by introducing shifted-discrete HSTs that are useful for performing the imaginary-time evolution of symmetry-broken trial wave functions. The formalism can be considered a generalization of the discrete HSTs in Ref. [23] or a compactification of

TABLE I. The staggered magnetization m of the two-dimensional Hubbard model at half filling in the thermodynamic limit. The staggered magnetization of the two-dimensional Heisenberg model from Refs. [61,62] is also shown. PBC stands for periodic boundary conditions, TABC stands for twist-averaged boundary conditions, and MBC stands for modified boundary conditions.

U/t	2	4	6	8	10	12	∞ (Heisenberg antiferromagnet)
AFQMC (this work)	0.120(1)	0.2340(2)	0.2815(2)	0.2991(2)	0.3046(1)	0.3067(2)	
AFQMC TABC [51]	0.119(4)	0.236(1)	0.280(5)	0.26(3)			
AFQMC TABC [52]	0.122(1)	0.2347(4)					
AFQMC PBC [36]		0.238(3)					
AFQMC MBC [63]	0.120(5)						
QMC Heisenberg model [61,62]							0.30743(1)

the shifted-contour auxiliary-field Monte Carlo formalism in Refs. [39,40] specialized to the on-site Hubbard interaction.

Properly chosen auxiliary fields can improve the efficiency of AFQMC simulations. The shifted real auxiliary fields can improve the acceptance ratio, while the shifted purely imaginary auxiliary fields can improve the average sign. The reason is that the shift in the real auxiliary field can stabilize the fluctuations of the modulus of the determinant, while the shift in the purely imaginary auxiliary field can stabilize the fluctuations of the phase of the determinant. However, even after the improvement, the average sign with the purely imaginary auxiliary field remains worse than the one obtained with the real auxiliary field for the doped cases. Therefore, in the presence of the sign problem, the real auxiliary field is still recommended for achieving longer imaginary-time propagations. On the other hand, at half filling with large U/t, the purely imaginary auxiliary field is dramatically more efficient than the real auxiliary fields for evaluating the staggered magnetization m.

In our approach, m_i and n_i in Eqs. (7) and (16) are arbitrary parameters that are not necessarily chosen as in Eq. (15) or in Eq. (24). For example, m_i (n_i) can be updated iteratively by the AFQMC expectation value of $\hat{n}_{i\uparrow} - \hat{n}_{i\downarrow}$ ($\hat{n}_{i\uparrow} + \hat{n}_{i\downarrow}$) with iterative simulations. This kind of scheme has already been employed to construct self-consistently an optimized trial wave function in the AFQMC [11]. Obviously, shifted-discrete HSTs can be used straightforwardly also in this case. Moreover, we expect that imaginary-time-dependent m_i or n_i could further improve the efficiency of the AFQMC, especially within the constrained path formalism. A study along this line is in progress [69].

It is also worth mentioning that the shifted-discrete HST is applicable straightforwardly to finite-magnetization cases, i.e., $N_\uparrow \neq N_\downarrow$, where N_σ is the number of electrons with spin σ. Indeed, in the half-filled case with $N_\uparrow \neq N_\downarrow$, where the sign problem is absent, our preliminary calculations have found that the shifted-real auxiliary field achieves better statistical samplings than the one without shift or the purely imaginary auxiliary field.

Finally, we remark on the d-wave superconducting order, which has not been considered in the present study. It is noteworthy that an early study on a t-t'-J model [70] showed that a stripe state with spatially oscillating d-wave superconductivity is favored around $1/8$ hole doping. Considering such an inhomogeneous superconductivity in a trial wave function might be of interest for a possible improvement of AFQMC simulations for doped Hubbard models with large U/t.

ACKNOWLEDGMENTS

The authors would like to thank S. Karakuzu, F. Becca, L. Fausto Tocchio, and T. Shirakawa for helpful discussions. K.S. acknowledges E. Küçükbenli and S. de Gironcoli for bringing his attention to Refs. [17,18]. Computations were done by using the HOKUSAI GreatWave and HOKUSAI BigWaterfall supercomputers at RIKEN under Projects No. G18007 and No. G18025. K.S. acknowledges support from the JSPS Overseas Research Fellowships. S.S. acknowledges support from the Simons Foundation.

APPENDIX A: IMPORTANCE SAMPLING

In this Appendix, we describe the importance sampling method within the AFQMC. An HST applied to $e^{-\Delta_\tau \hat{V}}$ transforms the quartic fermion-operator term into a quadratic one in its exponent at the cost of introducing the summation over auxiliary fields $\boldsymbol{s} = \{\boldsymbol{s}_l\} = \{s_{i,l}\}$ [see Eq. (9) or Eq. (18)]. Here, $\boldsymbol{s}$ ($\boldsymbol{s}_l$) is an NN_τ- (N-) dimensional vector, and the subscript i (l) denotes the site (imaginary-time) index. To describe the importance sampling method, it is crucial to explicitly write the auxiliary-field dependence in the imaginary-time evolution operator given in Eq. (6). For this purpose, we define an operator $\hat{B}_{\boldsymbol{s}_l}$ by

$$e^{-\frac{\Delta_\tau}{2}\hat{K}} e^{-\Delta_\tau \hat{V}} e^{-\frac{\Delta_\tau}{2}\hat{K}} = \prod_{i=1} \sum_{s_{i,l}=\pm 1} \hat{B}_{\boldsymbol{s}_l} \tag{A1}$$

and its product with respect to the imaginary-time index by $\hat{B}_{\boldsymbol{s}}(\beta, 0) = \prod_{l=1}^{N_\tau} \hat{B}_{\boldsymbol{s}_l}$. Then, the expectation value in Eq. (3) can be written as [up to the systematic error $O(\Delta_\tau^2)$]

$$\langle \hat{O} \rangle_\beta = \sum_{\boldsymbol{s}} P_{\beta,\boldsymbol{s}} \langle \hat{O} \rangle_{\beta,\boldsymbol{s}}, \tag{A2}$$

where $\sum_{\boldsymbol{s}} \cdots = \prod_{l=1}^{N_\tau} \prod_{i=1}^{N} \sum_{s_{i,l}=\pm 1} \cdots$, $P_{\beta,\boldsymbol{s}} = D_{\beta,\boldsymbol{s}} / \sum_{\boldsymbol{s}'} D_{\beta,\boldsymbol{s}'}$,

$$D_{\beta,\boldsymbol{s}} = \langle \Psi_{\mathrm{T}} | \hat{B}_{\boldsymbol{s}}(\beta, 0) | \Psi_{\mathrm{T}} \rangle, \tag{A3}$$

$$\langle \hat{O} \rangle_{\beta,\boldsymbol{s}} = \frac{\langle \Psi_{\mathrm{T}} | \hat{B}_{\boldsymbol{s}}(\beta, \beta/2) \hat{O} \hat{B}_{\boldsymbol{s}}(\beta/2, 0) | \Psi_{\mathrm{T}} \rangle}{\langle \Psi_{\mathrm{T}} | \hat{B}_{\boldsymbol{s}}(\beta, 0) | \Psi_{\mathrm{T}} \rangle}, \tag{A4}$$

$\hat{B}_{\boldsymbol{s}}(\beta, \beta/2) = \prod_{l=N_\tau/2+1}^{N_\tau} \hat{B}_{\boldsymbol{s}_l}$, and $\hat{B}_{\boldsymbol{s}}(\beta/2, 0) = \prod_{l=1}^{N_\tau/2} \hat{B}_{\boldsymbol{s}_l}$. In the last two equations, N_τ is assumed to be even for simplicity. If the determinant $D_{\beta,\boldsymbol{s}} = |D_{\beta,\boldsymbol{s}}| e^{i\theta_{\beta,\boldsymbol{s}}}$ is positive, $P_{\beta,\boldsymbol{s}}$ can be considered a probability distribution function. This is the case in which the sign problem is absent.

In general, $D_{\beta,\boldsymbol{s}}$ is complex, and the sign problem exists. In this case we rewrite Eq. (A2) as

$$\langle \hat{O} \rangle_\beta = \frac{\sum_{\boldsymbol{s}} \bar{P}_{\beta,\boldsymbol{s}} e^{i\theta_{\beta,\boldsymbol{s}}} \langle \hat{O} \rangle_{\beta,\boldsymbol{s}}}{\langle \mathrm{sign} \rangle_\beta}, \tag{A5}$$

where

$$\bar{P}_{\beta,\boldsymbol{s}} = \frac{|D_{\beta,\boldsymbol{s}}|}{\sum_{\boldsymbol{s}'} |D_{\beta,\boldsymbol{s}'}|} \tag{A6}$$

and

$$\langle \mathrm{sign} \rangle_\beta = \sum_{\boldsymbol{s}} \bar{P}_{\beta,\boldsymbol{s}} e^{i\theta_{\beta,\boldsymbol{s}}}. \tag{A7}$$

Now $\bar{P}_{\beta,\boldsymbol{s}}$ can be considered a probability distribution function because $\bar{P}_{\beta,\boldsymbol{s}} \geqslant 0$.

According to the Metropolis algorithm [71], the acceptance probability $\mathcal{P}_{\mathrm{acc}}$ of a proposed move from $\boldsymbol{s}$ to $\boldsymbol{s}'$ is given by

$$\mathcal{P}_{\mathrm{acc}}(\boldsymbol{s} \to \boldsymbol{s}') = \min(1, \mathcal{R}_{\mathrm{acc}}), \tag{A8}$$

where

$$\mathcal{R}_{\mathrm{acc}} = \frac{\bar{P}_{\beta,\boldsymbol{s}'}}{\bar{P}_{\beta,\boldsymbol{s}}} = \frac{|D_{\beta,\boldsymbol{s}'}|}{|D_{\beta,\boldsymbol{s}}|}. \tag{A9}$$

Equations (A8) and (A9) imply that the acceptance probability $\mathcal{P}_{\mathrm{acc}}$ remains large if the fluctuation of the modulus $|D_{\beta,\boldsymbol{s}}|$ of the determinant is reduced during the Monte Carlo simulation. On the other hand, Eq. (A7) implies that the average sign $\langle \mathrm{sign} \rangle_\beta$ remains large if the fluctuation of the phase $\theta_{\beta,\boldsymbol{s}}$ of the determinant is reduced during the Monte Carlo simulation.

APPENDIX B: DERIVATION OF SHIFTED-DISCRETE HSTs

In this Appendix, we derive Eqs. (10)–(12) and (19)–(21). First, we derive Eqs. (10)–(12), i.e., the shifted-discrete HST in the spin channel. Since the fermion density operator $\hat{n}_{i\sigma}$ is idempotent, i.e., $\hat{n}_{i\sigma}^2 = \hat{n}_{i\sigma}$, its exponential function is written as

$$e^{\alpha s \hat{n}_\sigma} = 1 + (e^{\alpha s} - 1)\hat{n}_\sigma. \tag{B1}$$

In this equation and hereafter, the site index i has been dropped for brevity. Then the right-hand side of Eq. (9) is given as

$$\begin{aligned}
&\frac{1}{2}\sum_{s=\pm 1} [1 + (e^{\alpha s} - 1)\hat{n}_\uparrow][1 + (e^{-\alpha s} - 1)\hat{n}_\downarrow] e^{-s\alpha m} \\
&= \cosh \alpha m + [\cosh \alpha(1-m) - \cosh \alpha m]\, \hat{n}_\uparrow \\
&\quad + [\cosh \alpha(1+m) - \cosh \alpha m]\, \hat{n}_\downarrow \\
&\quad + [2\cosh \alpha m - \cosh \alpha(1-m) - \cosh \alpha(1+m)]\hat{n}_\uparrow \hat{n}_\downarrow.
\end{aligned} \tag{B2}$$

The left-hand side of Eq. (9) is given as

$$\begin{aligned}
&C e^{-\Delta_\tau U \tilde{m}^2/2} e^{\frac{\Delta_\tau U}{2}(1-2\tilde{m})\hat{n}_\uparrow} e^{\frac{\Delta_\tau U}{2}(1+2\tilde{m})\hat{n}_\downarrow} e^{-\Delta_\tau U \hat{n}_\uparrow \hat{n}_\downarrow} \\
&= C e^{-\Delta_\tau U \tilde{m}^2/2} + C e^{-\Delta_\tau U \tilde{m}^2/2} \left[e^{\frac{\Delta_\tau U}{2}(1-2\tilde{m})} - 1 \right] \hat{n}_\uparrow \\
&\quad + C e^{-\Delta_\tau U \tilde{m}^2/2} \left[e^{\frac{\Delta_\tau U}{2}(1+2\tilde{m})} - 1 \right] \hat{n}_\downarrow \\
&\quad + C e^{-\Delta_\tau U \tilde{m}^2/2} \left[2 - e^{\frac{\Delta_\tau U}{2}(1-2\tilde{m})} - e^{\frac{\Delta_\tau U}{2}(1+2\tilde{m})} \right] \hat{n}_\uparrow \hat{n}_\downarrow.
\end{aligned} \tag{B3}$$

By comparing Eq. (B2) with Eq. (B3), we obtain Eqs. (10)–(12).

Next, we derive Eqs. (19)–(21), i.e., the shifted-discrete HST in the charge channel. As in Eq. (B1), we have

$$e^{i\alpha s \hat{n}_\sigma} = 1 + (e^{i\alpha s} - 1)\hat{n}_\sigma. \tag{B4}$$

Then the right-hand side of Eq. (18) is given as

$$\begin{aligned}
&\frac{1}{2}\sum_{s=\pm 1} [1 + (e^{i\alpha s} -)\hat{n}_\uparrow][1 + (e^{i\alpha s} - 1)\hat{n}_\downarrow] e^{-is\alpha n} \\
&= \cos \alpha n + [\cos \alpha(1-n) - \cos \alpha n)](\hat{n}_\uparrow + \hat{n}_\downarrow) \\
&\quad + [\cos \alpha(2-n) - 2\cos \alpha(1-n) + \cos \alpha n]\hat{n}_\uparrow \hat{n}_\downarrow.
\end{aligned} \tag{B5}$$

The left-hand side of Eq. (18) is given as

$$\begin{aligned}
&C e^{\Delta_\tau U \tilde{n}^2/2} e^{-\frac{\Delta_\tau U}{2}(1-2\tilde{n})(\hat{n}_\uparrow + \hat{n}_\downarrow)} e^{-\Delta_\tau U \hat{n}_\uparrow \hat{n}_\downarrow} \\
&= C e^{\Delta_\tau U \tilde{n}^2/2} + C e^{\Delta_\tau U \tilde{n}^2/2} \left[e^{-\frac{\Delta_\tau U}{2}(1-2\tilde{n})} - 1 \right] (\hat{n}_\uparrow + \hat{n}_\downarrow) \\
&\quad + C e^{\Delta_\tau U \tilde{n}^2/2} \left[e^{-\Delta_\tau U} e^{-\Delta_\tau U(1-2\tilde{n})} - 2e^{-\frac{\Delta_\tau U}{2}(1-2\tilde{n})} + 1 \right] \hat{n}_\uparrow \hat{n}_\downarrow.
\end{aligned} \tag{B6}$$

By comparing Eq. (B5) with Eq. (B6), we obtain Eqs. (19)–(21).

[1] J. P. F. LeBlanc, A. E. Antipov, F. Becca, I. W. Bulik, G. K.-L. Chan, C.-M. Chung, Y. Deng, M. Ferrero, T. M. Henderson, C. A. Jiménez-Hoyos, E. Kozik, X.-W. Liu, A. J. Millis, N. V. Prokof'ev, M. Qin, G. E. Scuseria, H. Shi, B. V. Svistunov, L. F. Tocchio, I. S. Tupitsyn, S. R. White, S. Zhang, B.-X. Zheng, Z. Zhu, and E. Gull (Simons Collaboration on the Many-Electron Problem), Phys. Rev. X **5**, 041041 (2015).

[2] B.-X. Zheng, C.-M. Chung, P. Corboz, G. Ehlers, M.-P. Qin, R. M. Noack, H. Shi, S. R. White, S. Zhang, and G. K.-L. Chan, Science **358**, 1155 (2017).

[3] G. Sugiyama and S. Koonin, Ann. Phys. (NY) **168**, 1 (1986).

[4] S. Sorella, S. Baroni, R. Car, and M. Parrinello, Europhys. Lett. **8**, 663 (1989).

[5] M. Imada and Y. Hatsugai, J. Phys. Soc. Jpn. **58**, 3752 (1989).

[6] F. Becca and S. Sorella, *Quantum Monte Carlo Approaches for Correlated Systems* (Cambridge University Press, Cambridge, 2017).

[7] S. Sorella, Y. Otsuka, and S. Yunoki, Sci. Rep. **2**, 992 (2012).

[8] Y. Otsuka, S. Yunoki, and S. Sorella, Phys. Rev. X **6**, 011029 (2016).

[9] Y. Otsuka, K. Seki, S. Sorella, and S. Yunoki, Phys. Rev. B **98**, 035126 (2018).

[10] H. Shi and S. Zhang, Phys. Rev. B **88**, 125132 (2013).

[11] M. Qin, H. Shi, and S. Zhang, Phys. Rev. B **94**, 235119 (2016).
[12] J. Xu, C.-C. Chang, E. J. Walter, and S. Zhang, J. Phys.: Condens. Matter **23**, 505601 (2011).
[13] S. Zhang, J. Carlson, and J. E. Gubernatis, Phys. Rev. B **55**, 7464 (1997).
[14] H.-H. Zhao, K. Ido, S. Morita, and M. Imada, Phys. Rev. B **96**, 085103 (2017).
[15] K. Ido, T. Ohgoe, and M. Imada, Phys. Rev. B **97**, 045138 (2018).
[16] A. S. Darmawan, Y. Nomura, Y. Yamaji, and M. Imada, Phys. Rev. B **98**, 205132 (2018).
[17] J. P. Perdew, A. Savin, and K. Burke, Phys. Rev. A **51**, 4531 (1995).
[18] D. J. Carrascal, J. Ferrer, J. C. Smith, and K. Burke, J. Phys.: Condens. Matter **27**, 393001 (2015).
[19] D. Tahara and M. Imada, J. Phys. Soc. Jpn. **77**, 114701 (2008).
[20] R. Rodríguez-Guzmán, K. W. Schmid, C. A. Jiménez-Hoyos, and G. E. Scuseria, Phys. Rev. B **85**, 245130 (2012).
[21] H. Shi, C. A. Jiménez-Hoyos, R. Rodríguez-Guzmán, G. E. Scuseria, and S. Zhang, Phys. Rev. B **89**, 125129 (2014).
[22] J. Hubbard, Phys. Rev. Lett. **3**, 77 (1959).
[23] J. E. Hirsch, Phys. Rev. B **28**, 4059 (1983).
[24] Y. Motome and M. Imada, J. Phys. Soc. Jpn. **66**, 1872 (1997).
[25] K. Held and D. Vollhardt, Eur. Phys. J. B **5**, 473 (1998).
[26] S. Sakai, R. Arita, and H. Aoki, Phys. Rev. B **70**, 172504 (2004).
[27] J. E. Han, Phys. Rev. B **70**, 054513 (2004).
[28] P. Broecker and S. Trebst, Phys. Rev. E **94**, 063306 (2016).
[29] D. R. Hamann and S. B. Fahy, Phys. Rev. B **47**, 1717 (1993).
[30] P. V. Buividovich and M. I. Polikarpov, Phys. Rev. B **86**, 245117 (2012).
[31] M. V. Ulybyshev, P. V. Buividovich, M. I. Katsnelson, and M. I. Polikarpov, Phys. Rev. Lett. **111**, 056801 (2013).
[32] M. Hohenadler, F. Parisen Toldin, I. F. Herbut, and F. F. Assaad, Phys. Rev. B **90**, 085146 (2014).
[33] H.-K. Tang, E. Laksono, J. N. B. Rodrigues, P. Sengupta, F. F. Assaad, and S. Adam, Phys. Rev. Lett. **115**, 186602 (2015).
[34] H.-K. Tang, J. N. Leaw, J. N. B. Rodrigues, I. F. Herbut, P. Sengupta, F. F. Assaad, and S. Adam, Science **361**, 570 (2018).
[35] G. G. Batrouni and R. T. Scalettar, Phys. Rev. B **99**, 035114 (2019).
[36] S. Karakuzu, K. Seki, and S. Sorella, Phys. Rev. B **98**, 201108(R) (2018).
[37] E. H. Lieb, Phys. Rev. Lett. **62**, 1201 (1989).
[38] T. Miyao, Ann. Henri Poincare **19**, 2543 (2018).
[39] N. Rom, D. Charutz, and D. Neuhauser, Chem. Phys. Lett. **270**, 382 (1997).
[40] N. Rom, E. Fattal, A. K. Gupta, E. A. Carter, and D. Neuhauser, J. Chem. Phys. **109**, 8241 (1998).
[41] R. Baer, M. Head-Gordon, and D. Neuhauser, J. Chem. Phys. **109**, 6219 (1998).
[42] S. Zhang and H. Krakauer, Phys. Rev. Lett. **90**, 136401 (2003).
[43] M. Motta, D. E. Galli, S. Moroni, and E. Vitali, J. Chem. Phys. **140**, 024107 (2014).
[44] D. Horn and M. Weinstein, Phys. Rev. D **30**, 1256 (1984).
[45] P. Weinberg and A. W. Sandvik, Phys. Rev. B **96**, 054442 (2017).
[46] H. F. Trotter, Proc. Am. Math. Soc. **10**, 545 (1959).
[47] M. Suzuki, Commun. Math. Phys. **51**, 183 (1976).
[48] J. E. Hirsch, Phys. Rev. B **31**, 4403 (1985).
[49] E. Y. Loh, J. E. Gubernatis, R. T. Scalettar, S. R. White, D. J. Scalapino, and R. L. Sugar, Phys. Rev. B **41**, 9301 (1990).
[50] H. J. Schulz, Phys. Rev. Lett. **65**, 2462 (1990).
[51] M. Qin, H. Shi, and S. Zhang, Phys. Rev. B **94**, 085103 (2016).
[52] S. Karakuzu, K. Seki, and S. Sorella, Phys. Rev. B **98**, 075156 (2018).
[53] J. E. Hirsch and S. Tang, Phys. Rev. Lett. **62**, 591 (1989).
[54] C. N. Varney, C.-R. Lee, Z. J. Bai, S. Chiesa, M. Jarrell, and R. T. Scalettar, Phys. Rev. B **80**, 075116 (2009).
[55] F. F. Assaad and I. F. Herbut, Phys. Rev. X **3**, 031010 (2013).
[56] D. Wang, Y. Li, Z. Cai, Z. Zhou, Y. Wang, and C. Wu, Phys. Rev. Lett. **112**, 156403 (2014).
[57] P. W. Anderson, Phys. Rev. **86**, 694 (1952).
[58] J. D. Reger and A. P. Young, Phys. Rev. B **37**, 5978 (1988).
[59] A. W. Sandvik, Phys. Rev. B **56**, 11678 (1997).
[60] M. Calandra Buonaura and S. Sorella, Phys. Rev. B **57**, 11446 (1998).
[61] A. W. Sandvik and H. G. Evertz, Phys. Rev. B **82**, 024407 (2010).
[62] F.-J. Jiang and U.-J. Wiese, Phys. Rev. B **83**, 155120 (2011).
[63] S. Sorella, Phys. Rev. B **91**, 241116(R) (2015).
[64] J.-Y. P. Delannoy, M. J. P. Gingras, P. C. W. Holdsworth, and A.-M. S. Tremblay, Phys. Rev. B **72**, 115114 (2005).
[65] C. Gros, Z. Phys. B **86**, 359 (1992).
[66] C. Gros, Phys. Rev. B **53**, 6865 (1996).
[67] T. Koretsune, Y. Motome, and A. Furusaki, J. Phys. Soc. Jpn. **76**, 074719 (2007).
[68] S. Karakuzu, L. F. Tocchio, S. Sorella, and F. Becca, Phys. Rev. B **96**, 205145 (2017).
[69] S. Sorella (unpublished).
[70] A. Himeda, T. Kato, and M. Ogata, Phys. Rev. Lett. **88**, 117001 (2002).
[71] N. Metropolis, A. W. Rosenbluth, M. N. Rosenbluth, A. H. Teller, and E. Teller, J. Chem. Phys. **21**, 1087 (1953).